INVERSE METHOD FOR THE ACOUSTIC SOURCE ANALYSIS OF AN AEROENGINE

Ulf Michel and Stefan Funke
DLR, German Aerospace Center
Institute of Propulsion Technology, Engine Acoustics
Müller-Breslau-Str. 8, 10623 Berlin

ABSTRACT

It is demonstrated that the source strengths and directivities of all sound sources of a high bypass ratio aeroengine can be determined from measurements in an open air test bed with a line array of microphones, which is laid out parallel to the engine axis in the geometric near field of the engine. The method is based on modelling the matrix of the cross-spectra of the microphones with a set of contributions from point monopoles assumed in positions along the engine axis and by solving the resulting set of linear equations for the unknown source strengths. The directivities of the sources are estimated by performing the analysis with a subarray of microphones, sliding from the front to the rear of the engine. The set of linear equations is solved with the side condition that the source strengths must be non-negative. The results demonstrate that the various sources of an aeroengine have a highly non-uniform directivity. The source positions are resolved with a separation of 0.4 wave lengths.

1 INTRODUCTION

Beamforming has become a standard method for the localisation of the sound sources on sound radiating objects. The results are presented in form of source maps, which are mathematically convolutions between the true source distributions and the point spread functions of all sources [12]. An estimation of the source strengths from these maps is possible only in rare cases, e.g., when the source positions are sufficiently separated spatially. Sources along a line or distributed over an area or over a source volume yield results that depend on the beam width of the point-spread function and on sidelobes and aliases. Additional problems arise when the source directivities are non-uniform. The consequence is that amplitudes of sound sources are very difficult to derive from beamforming maps.

The problem can be solved with deconvolution techniques. It is assumed that the point sources have a uniform directivity. The point spread functions of the array (or beamform maps) are calculated for every possible source position and for each narrow-band frequency of interest. The source levels of the unknown sources have then to be determined with a least square fit for the difference between the measured beamform map and the estimate for the sum of point sources.

This deconvolution procedure yields huge and often badly conditioned matrices. Special iterative procedures are required to solve them with the side condition that only positive source levels are permitted.

A first procedure proposed to solve the complete inverse problem for microphone arrays was published by Brühl and Röder (2000) [7]. Brooks and Humphreys (2004-2006) [3, 4, 5, 6] developed a solution procedure called DAMAS and Dougherty (2005) [8] proposed a simplification DAMAS2, where a common point spread function is assumed for all sources as an approximation with the objective of increasing the computational speed. Various deconvolution methods are compared by Ehrenfried and Koop (2007) [9]. The deconvolution of the beamform maps of moving sources is more difficult, because the sidelobes of the point spread function have a different frequency than the main lobe. Guérin et al. (2006) [11] proposed a method to compute an average point spread function for the broadband noise of moving sources with the condition that the narrow-band levels of the sources are constant in neighbouring frequency bands.

Sijtsma [15] developed a different approach (CLEAN-SC) to solve the inverse problem. He makes use of the fact that the sidelobes in the beam pattern of a source are spatially correlated with the main lobe while the main lobes of other sources are uncorrelated. CLEAN-SC iteratively removes the part of the source plot which is spatially coherent with the peak source and attributes it to a source of known strength. The resulting procedure is computationally rapid in contrast to the deconvolution methods.

Blacodon and Élias [1, 2] propose a different method for the determination of the source strengths of assumed sources. The method is based on modelling the cross-spectral matrix of the microphone signals. Instead of determining the sources such that the beamform maps are best approximated, Blacodon and Élias determine the sources for a best approximation of the cross-spectral matrix. They generate a cross-spectral matrix for each possible point source position assuming a uniform directivity of the sources. The amplitudes of the sources are then determined with a least square fit between the modelled and the measured cross-spectral matrix. The beamforming map is not required for their method.

The objective of this paper is the analysis of the sound sources of an aeroengine during noise tests on an open air test bed. A proven method to accomplish this is the polar correlation technique of Fisher, Harperbourne and Glegg (1977) [10]. The signals of a microphone array installed on a polar arc around the exhaust nozzle of the engine are evaluated in this technique. The technique yields the strengths of point sources on the engine and constants for a parametric model of jet mixing noise. A prediction of the far-field radiation is not possible from these results because the directivity of the sources is not known for all emission angles.

It is the purpose of the present paper to develop a method that is based on a line array of microphones, which permits the determination not only of the source strengths but also of the directivities of the sources. The method of Blacodon and Élias [2] is used as a starting point but extended to include the directivities of the sources. The method is described in section 2. The procedure is then applied to data that were acquired during a test of a modern large bypass ratio engine in an outdoor test facility. Results of a narrowband analysis in frequency bands ranging from 100 Hz to 3150 Hz are shown in section 3. Results for one-third octave bands are shown in section 4. The directivities in narrowbands are used to compute the source distributions along the engine axis in one-third octave bands for three emission angles 60, 90, and 120 deg relative to the inlet. Finally, the directivities are predicted for one-third octave bands in the positions of the far-field microphones, which are located on a radius with 45.7 m around the centre of the test rig.

2 METHODS

2.1 Set-up of microphone array

The microphone positions are shown in figure 1 in relation to the location of the engine. The distance between the line array and the engine centre-line is about 9.5 m. The microphones of the array are in the acoustic far field of the sources but in the geometric near field of the whole source distribution. The axial spacing of the microphones is 217 mm in the centre. In front of the intake and behind the primary nozzle the spacing increases such that the emission angle changes by 1.25 deg between two microphones. The emission angle of the most forward microphone is 25 deg relative to the inlet, the angle of the most rearward one is 146.25 deg relative to the nozzle.

It is assumed that acoustic sources are located in known positions along the centerline of the tested aeroengine. The spacing between the sources is chosen to be 0.4λ, where λ is the wavelength of the narrowband or of the reference frequency of the one-third octave band. The source positions in the analysis results of this paper started at 2.24 m in front of the intake and ended at 9000 m/(f/Hz) downstream of the primary nozzle. The downstream positions are limited to -30 m. The resulting number of sources is 27 for 100 Hz and 273 for 3150 Hz.

128 microphones were installed, of which $M = 127$ usable signals were available for the analysis. The microphone signals were sampled with a frequency of 32786 Hz. The available signal length was 30 seconds and the FFT time segment length was chosen $T = 0.25$ s with 8192 samples, yielding a frequency interval of $\Delta f = 4.002$ Hz. The fast Fourier transforms (FFT) were performed with a Hanning window and an 50% overlap, resulting in an averaging over 240 time segments and a subsequently statistically very stable cross-spectral matrix. Each frequency band consists of a matrix $C_{m,n}$ of M by M complex values. The Matrix is Hermitian, $C_{m,n} = C^*_{n,m}$, where the * indicates the conjugate complex element.

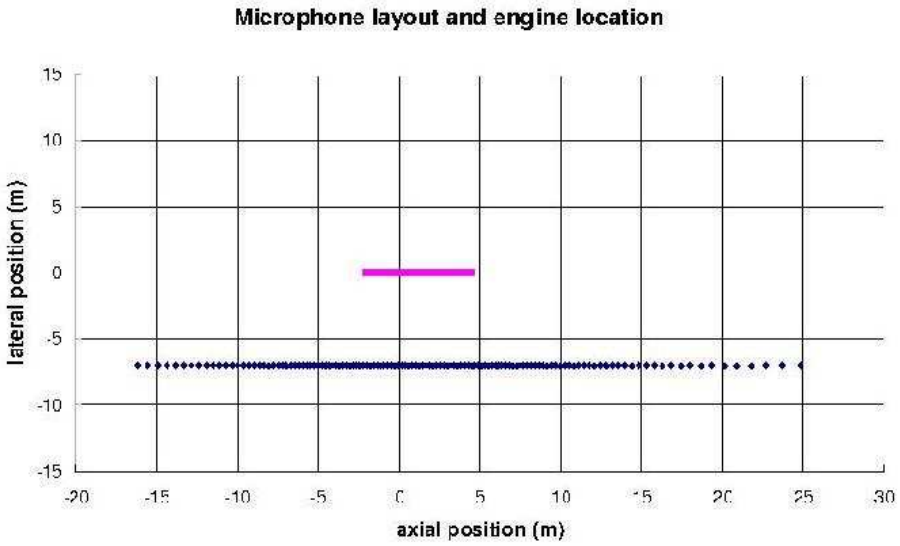

Figure 1: Positions of the line array of microphones and of the aeroengine. The line array is longer in the forward arc ($x > 0$) than in the rear arc. The jet is on the left side of the figure and extends substantially past the left end of the array.

The engine was investigated in a range of power settings from almost idle to maximum power. The results shown in this paper are for a test point just below the appearance of tones at multiples of the fan shaft frequency.

2.2 Evaluation of the source distribution

The measured matrix $C_{m,n}$ is compared with a modelled matrix consisting of the sum of the matrices generated by each of the J unknown sources. Blacodon and Élias [2] assume a uniform

directivity for each source, which yields the following equation for the modelled cross-spectral matrix,

$$C_{m,n}^{\text{mod}} = \sum_{j=1}^{J} g_{m,j} S_j g_{n,j}^*, \tag{1}$$

where

$$g_{m,j} = \mathrm{e}^{\mathrm{i}kr_{j,m}}/r_{j,m} \tag{2}$$

are the steering vectors between the source positions ξ_j ($j = 1 \ldots J$) and the microphone positions x_m ($m = 1 \ldots M$). These vectors determine the phase of the cross spectra.

$$r_{j,m} = |x_m - \xi_j| \tag{3}$$

The goal is to determine the strengths S_j of the J sources such that the mean square error $F(S)$ between the measured and the modelled matrix becomes a minimum.

$$F(S) = \sum_{m,n=1}^{M} \left| C_{m,n} - \sum_{j=1}^{J} g_{m,j} S_j g_{n,j}^* \right|^2 \tag{4}$$

The condition for a minimum of $F(S)$ is

$$\frac{\partial F(S)}{\partial S_j} = 0, \qquad \text{for} \qquad 1 \le j \le J \tag{5}$$

which yields the set of J linear equations

$$\sum_{j=1}^{J} V_{i,j} S_j = U_i, \qquad \text{for} \qquad 1 \le i \le J. \tag{6}$$

U_i and $V_{i,j}$ are given by [2]

$$U_i = \sum_{m,n=1}^{M} g_{m,i} C_{m,n} g_{n,i}^*, \tag{7}$$

$$V_{i,j} = \left| \sum_{m=1}^{M} g_{m,i} g_{m,j}^* \right|^2. \tag{8}$$

The exact solution of equation (6) may yield a solution vector S_j with negative source levels for some of the source positions s_j. In order to ensure that all S_j are positive, Blacodon and Élias replace S_j in equation (4) by α_j^2 and search for the minimum of equation

$$F(\alpha) = \sum_{m,n=1}^{M} \left| C_{m,n} - \sum_{j=1}^{J} g_{m,j} \alpha_j^2 g_{n,j}^* \right|^2. \tag{9}$$

This is a nonlinear optimisation problem, which is solved by Blacodon & Élias with a procedure published by Shanno & Phua [14].

Instead of solving the nonlinear problem, one can alternatively solve the linear problem (6) by considering the side condition that the S_j must be real and non-negative. This procedure was applied for the results shown in this paper. A slightly modified version of the Gauss-Seidel procedure of Brooks & Humphreys [3] was applied. The modifications consider that a linear set of complex rather than real equations has to be solved and that the solution must be real.

One advantage of positioning the line array in the geometric near field is that the solution of equation (5) does generally pose no problem. No regularisation of the matrix is necessary.

2.3 Consideration of directivities of the sources

It is known that the radiation from the intake and the nozzles is highly directive, violating the assumption of uniform directivity in equation (4). Jet noise also has a distinctive directivity.

Jet noise is a volume source, in which the sources are correlated over at considerable volume. It might be questionable if these sources can be described in terms of independent point sources. However, it was shown by Michel (2007) [13] that the power-spectral density of jet noise in the acoustic far field can be expressed as an integral over uncorrelated source volume elements. The effects of source interference are considered by an interference integral, which has a strong directivity. It can be concluded that jet noise sources can only be modelled correctly if their directivities due to source interference are considered.

It was already proposed by Blacodon & Élias [2] to determine the directivity of the sources by changing the position of the microphone array. However, a uniform directivity is still assumed for all microphones of the array in each array position. The same procedure is applied here to yield a first approximation for the directivity. A subarray of 21 microphones is used in all results presented in this paper. This array is moved in increments of 5 microphone positions over the whole length of the line array, yielding 22 subarrays and 22 directivity values for each of the J sources. The directivity value for any required angle is obtained by interpolation. Outside the available range of angles the directivity values are assumed to be constant. The results for the far-field directivities shown in section 4.2 were computed with this procedure.

2.4 Determination of the directivities of the sources

The inclusion of the directivities of the sources in equation (4) yields

$$F(D) = \sum_{m,n=1}^{M} \left| C_{m,n} - \sum_{j=1}^{J} g_{m,j} D_{m,j} D_{n,j} g_{n,j}^{*} \right|^2 , \tag{10}$$

where $D_{m,j}^2$ is the directivity of the source intensity of source j toward microphone m. A minimum of $F(D)$ requires that

$$\frac{\partial F(D)}{\partial D_{m,j}} = 0, \qquad (m = 1 \ldots M,\ j = 1 \ldots J) \tag{11}$$

The optimisation problem of finding a minimum of $F(D)$ is a nonlinear one and requires a suitable numerical procedure like the one of Shanno & Phua [14]. The solution procedure must either observe a side condition that $F(D)$ is real and positive or the directivities $D_{m,j}$ have to be replaced by $D_{m,j} = \beta_{m,j}^2$.

While the number of unknowns was J in equation (5) it has now increased to MJ in equation (11). In the case of $M = 127$ and $J = 100$ we have 12700 unknowns. The total number of independent real values in the cross-spectral matrix is M^2, which would in principle allow to determine the directivities of $J \leq M$ sources. However, in the case of high frequencies, we have $J > M$. As a consequence of the large number of unknowns, the problem is ill-conditioned. We need additional conditions to make the solution possible. One side-condition is that all solutions $D_{m,j}$ must be real and positive, which must be assured by the iterative solution procedure. In addition one may assume that the directivities of neighbouring source positions are very similar, at least in the jet source region. This can be described by the following two functions

$$G_1(D) = \sum_{j=1}^{J} \sum_{m=2}^{M-1} \left(D_{m,j} - 0.5(D_{m-1,j} + D_{m+1,j}) \right)^2 \tag{12}$$

$$G_2(D) = \sum_{m=1}^{M} \sum_{j=2}^{J-1} \left(D_{m,j} - 0.5(D_{m,j-1} + D_{m,j+1}) \right)^2 \tag{13}$$

Instead of finding a minimum of $F(D)$ a minimum has to be determined for

$$G(D) = F(D) + \sigma_1 G_1(D) + \sigma_2 G_2(D) \tag{14}$$

where the slack variables σ_1 and σ_2 have to be optimised experimentally. A large value of σ_1 would force a more uniform directivity, a large value of σ_2 smooths the axial variation of the source strengths. The solution according to section 2.3 would serve as the initial estimate.

Equation (14) has not been used for the results shown in this paper.

3 NARROWBAND RESULTS

The source distributions are calculated for subarrays consisting of 21 microphones. Figure 2 shows the results for the frequency $f = 100$ Hz with a bandwidth of $\Delta f = 4$ Hz. The results of three subarrays are shown. The subarray consisting of microphones 21 to 41 is located in front of the inlet in the forward arc of the engine, the subarray of microphones 51 to 71 is located on the side of the engine, and the subarray consisting of microphones 101 to 121 is located in the rear arc of the engine. The black solid vertical lines indicate the axial positions of the inlet and the secondary and primary nozzles of the engine. The blue dashed vertical lines indicate the limits of the subarray used to create the figure.

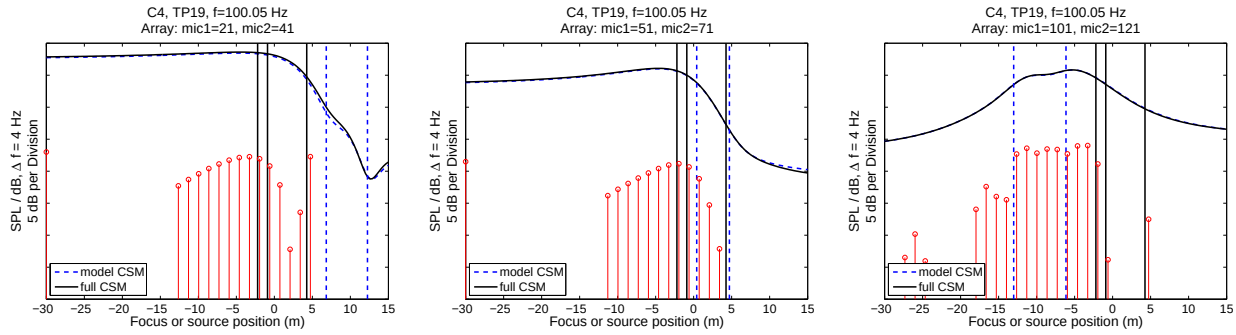

(a) forward arc (b) centre (c) rear arc

Figure 2: Source distribution for narrowband at $f = 100$ Hz, $\Delta f = 4$ Hz.

The vertical stem lines indicate the strengths of the sources in these positions. Please note that one source is located at $x = -30$ m in the subplots 2(a) and 2(b). This is likely a result of the assumption of a uniform directivity in the modelling of the cross-spectral matrix for the subarray. It can be seen that the strengths change substantially between the three subarrays.

Each figure contains a solid black curve, which shows the beamforming result based on the microphones of the subarray. The dashed blue curve is the beamforming result based on the modelled cross-spectral matrix. The difference between the two curves is almost negligible. By comparing the distribution of the sources with the beamform result it can be seen that the new procedure has a far superior source resolution capability than the beamform map at this low frequency. Almost all sources for $f = 100$ Hz are located in the jet region. A considerable source can be seen in the inlet only in the forward arc.

The corresponding results for a frequency $f = 200$ Hz are shown in Figure 3. The results for the angles in the forward and rear arcs may be influenced by parallax errors. The inlet cannot be seen from the rear and the emitted sound has to propagate around the edge of the intake. As a consequence the source position of the sound emitted from the inlet is seen in the front of the engine in Figure 3(c) when viewed from the rear arc. The same is true for the bypass nozzle. The part of the bypass ring nozzle that is located on the opposite side of the engine with respect to the microphone array is obstructed by the core nozzle. The source location is seen further forward at larger x-values as a consequence . In spite of the sources at the inlet position, most sources for

$f = 200$ Hz are located in the jet region. The two beamform distributions of the measured and the simulated cross-spectral matrix are seen to be almost identical. The dynamic range of these curves is more than 20 dB in the forward arc, nevertheless, the source locations cannot be determined reliably, not to mention the source levels.

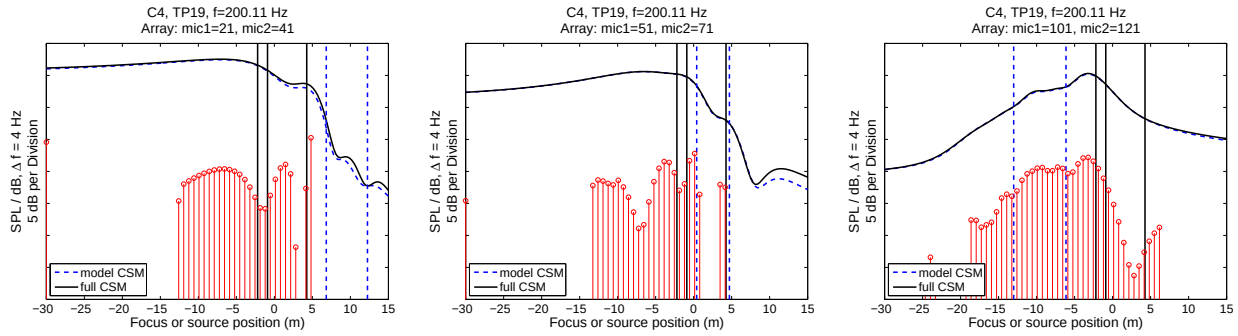

(a) forward arc (b) centre (c) rear arc

Figure 3: Source distribution for narrowband at $f = 200$ Hz, $\Delta f = 4$ Hz.

The corresponding results for a frequency $f = 400$ Hz are shown in Figure 4. The distance $\Delta\xi$ between adjacent sources gets smaller because $\Delta\xi$ is assumed to be proportional to the wave length λ. A strong source can be seen in the inlet and the exit of the bypass nozzle for all three angles.

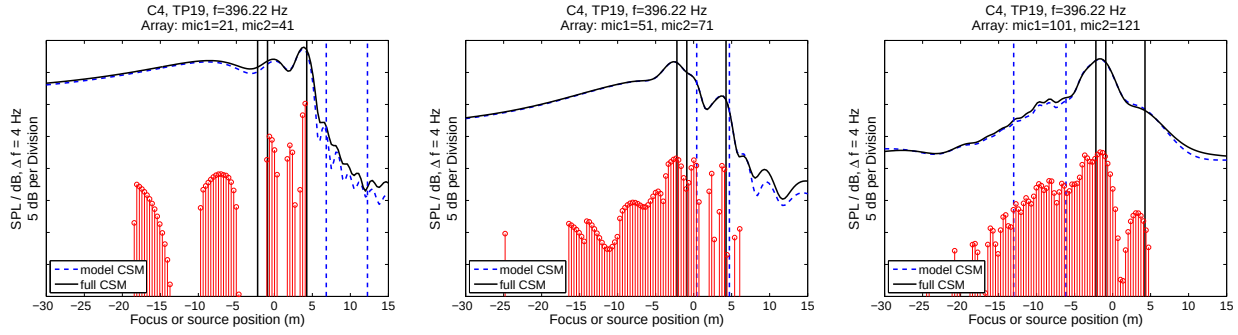

(a) forward arc (b) centre (c) rear arc

Figure 4: Source distribution for narrowband at $f = 400$ Hz, $\Delta f = 4$ Hz.

The corresponding results for a frequency $f = 800$ Hz are shown in Figure 5. The inlet is seen to emit sound primarily into the forward arc. The bypass and core nozzles dominate the radiation into the rear arc. The beamform curves start to show aliases for $x > 12$ m in the forward arc and for $x < -13$ m in the rear arc.

The corresponding results for a frequency $f = 1600$ Hz are shown in Figure 6. The aliases in the beamform maps move toward the engine. Both nozzles can be distinguished in Figure 6(b). Their source positions are slightly moved downstream due to the convection effect of the jet flow. An additional source can be seen on the engine at approximately $x = 1$ m. The jet and the two nozzles hardly contribute to the sound radiation in the forward arc.

The corresponding results for a frequency $f = 3150$ Hz are shown in Figure 7. It can be seen that the sources can still be localised at this high frequency. Figure 6(b) shows that the radiation to the side is dominated by the region between the primary and secondary nozzles. The rear arc is dominated by the secondary nozzle, which is seen at a slightly shifted position due the parallax effect already discussed on page 6.

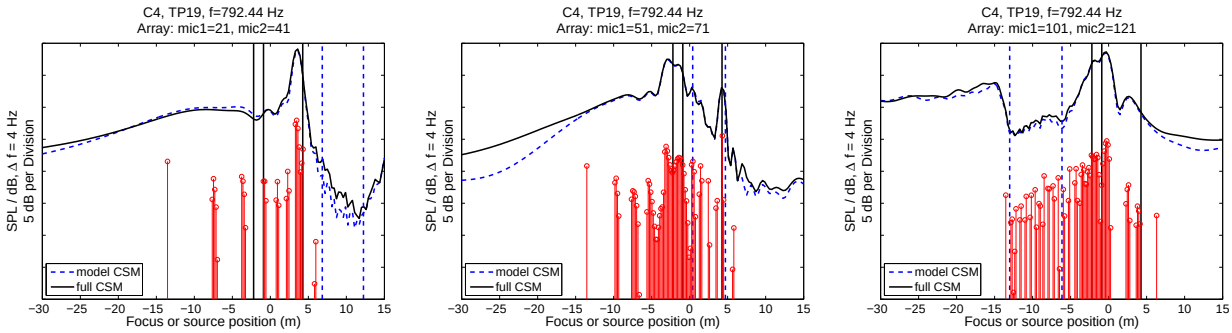

(a) forward arc (b) centre (c) rear arc

Figure 5: Source distribution for narrowband at $f = 800$ Hz, $\Delta f = 4$ Hz.

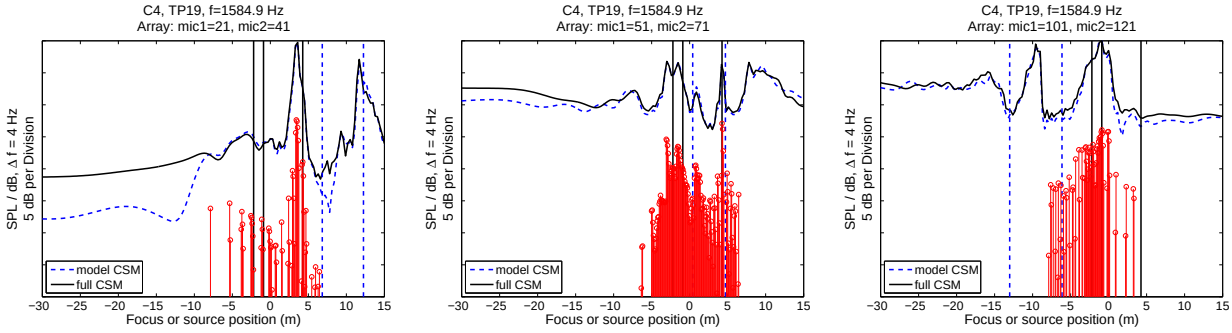

(a) forward arc (b) centre (c) rear arc

Figure 6: Source distribution for narrowband at $f = 1600$ Hz, $\Delta f = 4$ Hz.

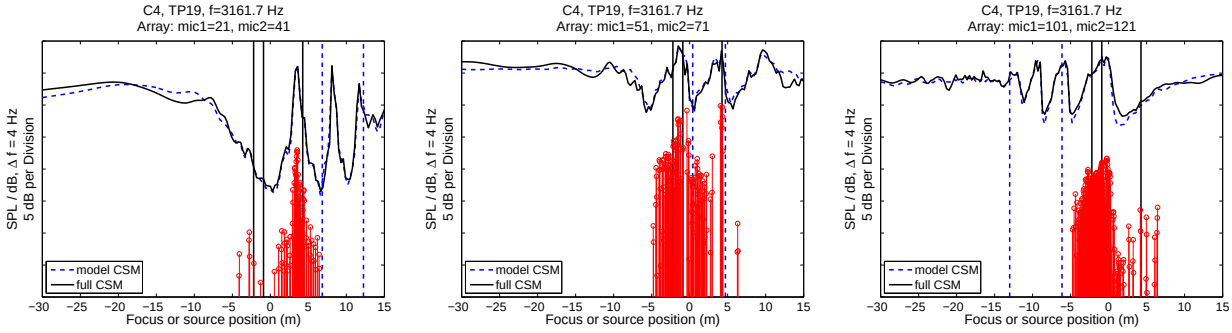

(a) forward arc (b) centre (c) rear arc

Figure 7: Source distribution for narrowband at $f = 3150$ Hz, $\Delta f = 4$ Hz.

4 ONE-THIRD OCTAVE BANDS IN FAR FIELD

4.1 Source distribution as function of emission angle

The source distributions along the engine centreline are now shown for the one-third octave bands 100 Hz, 200 Hz, 400 Hz, 800 Hz, 1600 Hz and 3150 Hz as seen from the positions of the far-field microphones at 60 degrees, 90 degrees, and 120 degrees located in a distance of 45.7 m. The sources of all narrowbands of a one-third octave band are summed up and shown. The positions of the engine inlet (not visible in figure 8) and the two nozzles are indicated by vertical red lines. The majority of the sources for 100 Hz are located in the jet region. This is true for all three angles. Please note the large dynamic range of about 20 dB between the loudest and quietest sources.

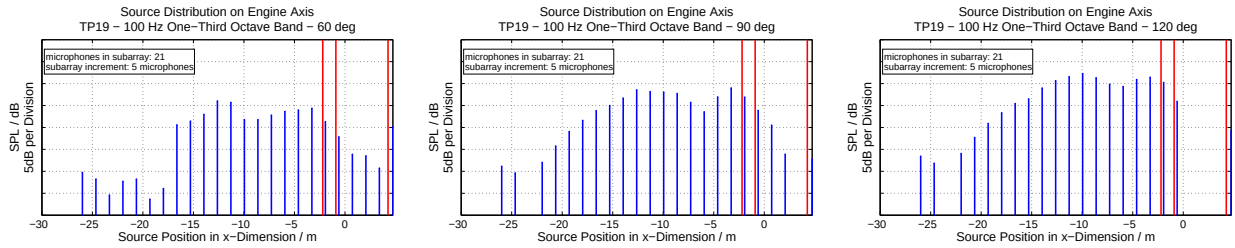

(a) 60 deg (b) 90 deg (c) 120 deg

Figure 8: Source distribution of one-third octave band 100 Hz as seen from the far-field microphones at emission angles 60 deg, 90 deg, and 120 deg.

The situation has hardly changed for 200 Hz. It is interesting to see that the source region extends to 25 m downstream of the nozzle, where the source strength has reduced by about 20 dB. Please recall that the line array ended at $x = -17$ m (figure 1), which indicates that the source levels in the jet far downstream are determined by extrapolation as explained at the end of section 2.3 on page 5.

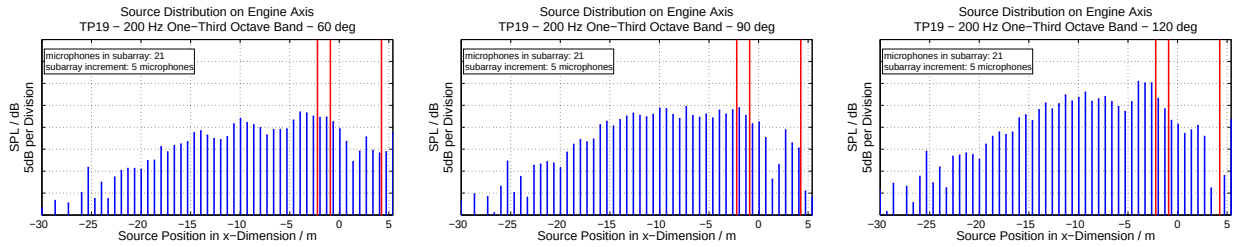

(a) 60 deg (b) 90 deg (c) 120 deg

Figure 9: Source distribution of one-third octave band 200 Hz as seen from the far-field microphones at emission angles 60 deg, 90 deg, and 120 deg.

At 400 Hz we start to see a substantial noise emission from the inlet toward 60 deg. The source strength for 120 deg peaks at the location of the two nozzles.

For 800 Hz the radiation from the inlet becomes the most prominent one for 60 deg. The sound appears to be emitted from a position downstream of the axial inlet position, more toward the fan face. The two other angles are dominated by the radiation from the two nozzles.

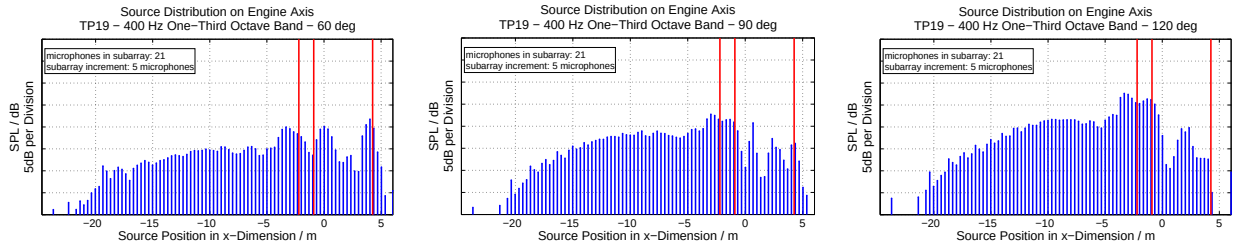

(a) 60 deg (b) 90 deg (c) 120 deg

Figure 10: Source distribution of one-third octave band 400 Hz as seen from the far-field microphones at emission angles 60 deg, 90 deg, and 120 deg.

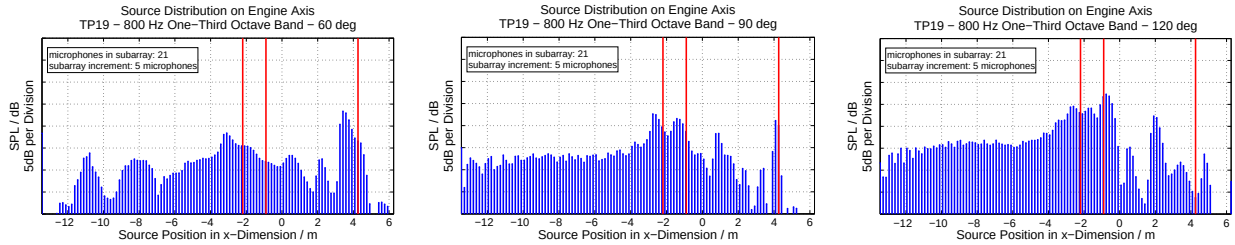

(a) 60 deg (b) 90 deg (c) 120 deg

Figure 11: Source distribution of one-third octave band 800 Hz as seen from the far-field microphones at emission angles 60 deg, 90 deg, and 120 deg.

For 1600 Hz and 60 deg the peak radiation is from a position downstream of the intake. Both nozzles dominate at 90 deg. The rear arc is dominated by the two nozzles and the region between the two nozzles.

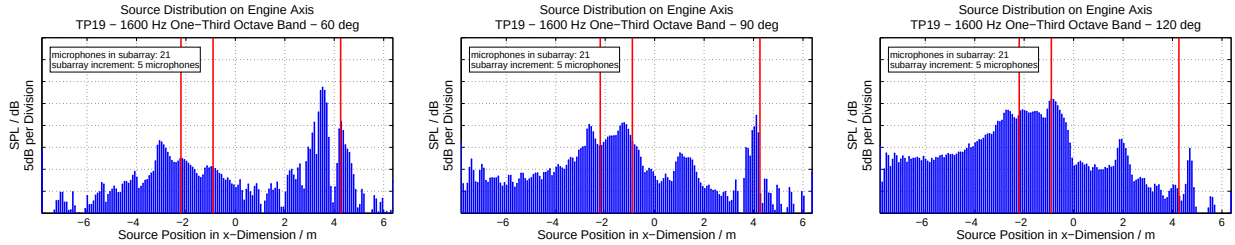

(a) 60 deg (b) 90 deg (c) 120 deg

Figure 12: Source distribution of one-third octave band 1600 Hz as seen from the far-field microphones at emission angles 60 deg, 90 deg, and 120 deg.

The radiation into the forward arc in the one-third octave band of 3150 Hz is dominated by the position $x = 3$ m downstream of the intake toward the fan face. The intake dominates for 90 deg and the two nozzles for 120 deg.

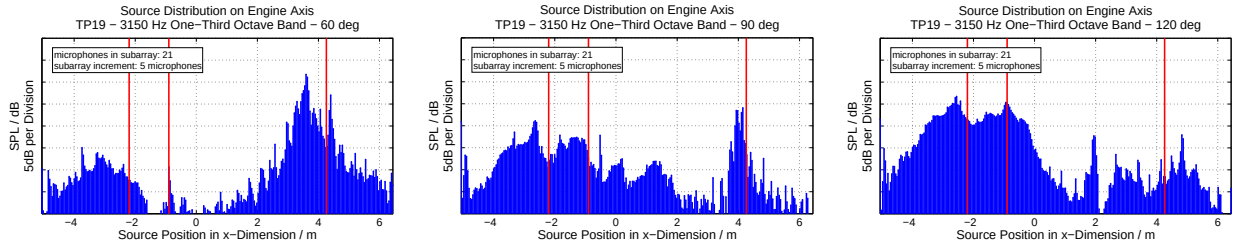

(a) 60 deg (b) 90 deg (c) 120 deg

Figure 13: Source distribution of one-third octave band 3150 Hz as seen from the far-field microphones at emission angles 60 deg, 90 deg, and 120 deg.

4.2 Directivity in far field

Using the directivity of each individual source, one can compute the sound radiation to any position in the far field. The predictions for the positions of the far-field microphones located in a radial distance of 45.7 m are compared in the following figures for the three microphones at 60 degrees, 90 degrees, and 120 degrees with the experimental data. The directivity of the one-third octave bands of 100 Hz, 200 Hz, and 400 Hz are shown in Figures 14(a), 14(b), and 14(c), respectively. The valid range of the predictions is indicated by two vertical red lines. This is the range, where directivities are available for all sources. It can be seen that the predictions are too low by between 0 dB and 1.5 dB.

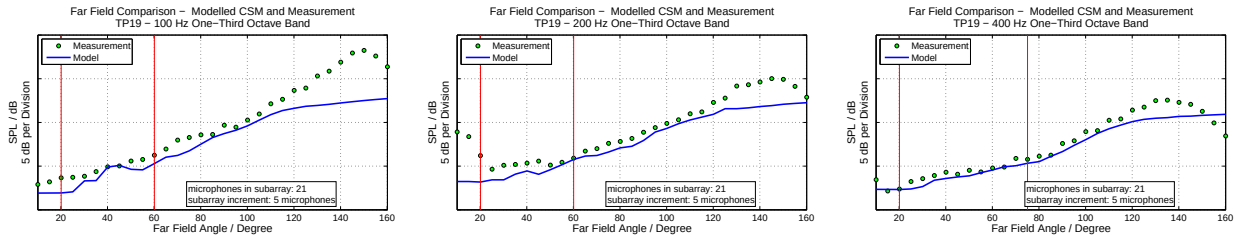

(a) 100 Hz (b) 200 Hz (c) 400 Hz

Figure 14: Far-field directivity for one-third octave bands 100 Hz, 200 Hz, and 400 Hz in comparison with measured results.

The results for the higher frequencies 800 Hz, 1600 Hz, and 3150 Hz are shown in Figures 15(a), 15(b), and 15(c), respectively. While the predictions for 800 Hz and 1600 Hz are very good, the predicted directivity for 3150 Hz has its minimum shifted to a slightly smaller angle than the corresponding measurement. None of the refraction dimples in the rear arc are predicted correctly because the microphone array was too short in the downstream direction.

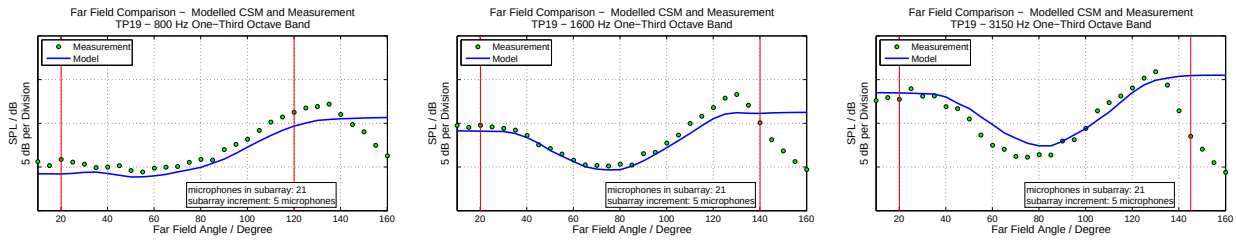

(a) 800 Hz (b) 1600 Hz (c) 3150 Hz

Figure 15: Far-field directivity for one-third octave bands 800 Hz, 1600 Hz, and 3150 Hz in comparison with measured results.

5 CONCLUSIONS

The initial results of a new source localisation procedure are very promising. The distribution of the sources appears physically realistic, and the levels exhibit a large dynamic range. The predicted directivities for far-field positions agree very well with experimental data. So far, the directivities are only derived from the results of a sliding subarray. The analysis in each subarray is based on the assumption of a uniform directivity of the sources. A further improvement can be expected when the directivities of the sources are included in the modelling of the cross-spectral matrix as proposed in section 2.4.

The new method provides the directivities of all sources of a jet engine and is superior in this respect to the polar arc correlation method [10]. The maximum analysis frequency with the current microphone layout is about 3 kHz. Future tests should be performed with an array that extends further downstream to about $x = -30$ m for a better modelling of the low-frequency portion of jet noise. This would increase the numbers of microphones in the array to about 140. Raising the maximum frequency of the analysis to 4 kHz would require a further increase of the number of microphones to about 180.

REFERENCES

[1] D. Blacodon and G. Élias. Level estimation of extended acoustic sources using an array of microphones. AIAA Paper 2003-3199, 2003. 9th AIAA/CEAS Aeroacoustics Conference, Hilton Head, South Carolina, May 12-14, 2003.

[2] D. Blacodon and G. Élias. Level estimation of extended acoustic sources using a parametric method. *Journal of Aircraft*, 41:1360–1369, 2004.

[3] T. Brooks and W. Humphreys. A deconvolution approach for the mapping of acoustic sources (DAMAS) determined from phased microphone arrays. AIAA Paper 2004-2954, 2004. 10th AIAA/CEAS Aeroacoustics Conference, Manchester, Great Britain, May 10-12, 2004.

[4] T. Brooks and W. Humphreys. Three-dimensional applications of DAMAS methodology for aeroacoustic noise source definition. AIAA Paper 2005-2960, 2005. 11th AIAA/CEAS Aeroacoustics Conference, Monterey, California, May 23-25, 2005.

[5] T. Brooks and W. Humphreys. A deconvolution approach for the mapping of acoustic sources (DAMAS) determined from phased microphone array. *J. Sound Vib.*, 294:856–879, 2006.

[6] T. Brooks and W. Humphreys. Extension of DAMAS phased array processing for spatial coherence determination (DAMAS-C). AIAA Paper 2006-2654, 2006. 12th AIAA/CEAS Aeroacoustics Conference, Cambridge, Massachusetts, May 8-10, 2006.

[7] S. Brühl and A. Röder. Acoustic noise source modelling based on microphone array measurements. *J. Sound Vib.*, 231:611–617, 2000.

[8] R. P. Dougherty. Extensions of DAMAS and benefits and limitations of deconvolution in beamforming. AIAA Paper 2005-2961, 2005. 11th AIAA/CEAS Aeroacoustics Conference, Monterey, California, May 23-25, 2005.

[9] K. Ehrenfried and L. Koop. Comparison of iterative deconvolution algorithms for the mapping of acoustic sources. *AIAA Journal*, pages 1584–1595, 2007.

[10] M. J. Fisher, M. Harper-Bourne, and S. A. L. Glegg. Jet engine noise source location: The polar correlation technique. *J. Sound Vib.*, 51:23–54, 1977.

[11] S. Guérin, C. Weckmüller, and U. Michel. Beamforming and deconvolution for aerodynamic sound sources in motion. 1st Berlin Beamforming Conference. 21-22 November 2006, 2006.

[12] Don H. Johnson and Dan E. Dudgeon. *Array Signal Processing, Concepts and Techniques*. P T R Prentice Hall, Englewood Cliffs, 1993.

[13] U. Michel. Influence of source interference on the directivity of jet noise. AIAA Paper 2007-3648, 2007. 13th AIAA/CEAS Aeroacoustics Conference, Rome, Italy, May 21-23, 2007.

[14] D. F. Shanno and K. H. Phua. Remark on "Algorithm 500: Minimization of unconstrained multivariate functions [e4]". *ACM Trans. Math. Softw.*, 6(4):618–622, 1980.

[15] P. Sijtsma. CLEAN based on spatial source coherence. AIAA Paper 2007-3436, 2007. 13th AIAA/CEAS Aeroacoustics Conference, Rome, Italy, May 21-23, 2007.